Mine Water Environ (2015) 34:231–240
DOI 10.1007/s10230-014-0311-7

TECHNICAL ARTICLE

Mesoporous Silica Nanoparticles for the Adsorptive Removal of Cu(II), Mn(II), and U(VI) from Acid Mine Drainage

Anita Etale · Hlanganani Tutu · Deanne C. Drake

Received: 8 May 2014 / Accepted: 8 October 2014 / Published online: 26 October 2014

Abstract The adsorption of Cu(II), Mn(II), and U(VI) ions by mesoporous silica nanoparticles (NPs) was investigated by batch experiments to assess the potential using NPs to remediate acid mine drainage (AMD) contaminated water. Adsorption reactions were found to be rapid, attaining equilibrium within 5 min for Cu and less than a minute for Mn and U. Calculated adsorption rates based on the pseudo-second order model ($R^2 = 0.99$) showed that Mn adsorption was >3 times faster than Cu and 7 times faster than U. Adsorption increased with pH and temperature, and $\Delta G°$ and $\Delta H°$ values indicate that the process was spontaneous and endothermic. Isotherm data were best described by the Freundlich and Temkin models ($R^2 = 0.99$), with chemisorption responsible for the removal of Cu and Mn, and adsorption and precipitation for U removal. Importantly, Fe^{3+}, Mn, and SO_4^{2-} ions increased adsorption from 52, 56, and 49 % to 77, 66, and 76 % for Cu, Mn, and U, respectively. Cu removal was, however, inhibited in 1:2 Cu:Mn solutions. NPs were then applied to actual AMD-contaminated ground and surface water. As in simulated AMD, adsorption was higher for Mn than Cu and removal efficiencies of up to 60 % for Mn and 34 % for Cu were attained. These NPs therefore offer an alternative for Mn removal that precludes pH adjustment and the copious amounts of lime required for that. Importantly, they can be used for cost-effective treatment of AMD-contaminated water.

Keywords Adsorption · Metal pollution · Gold mining · Witwatersrand · AMD remediation

Introduction

In addition to its economic benefits, mining often causes significant environmental damage (Nriagu 1988). Gold mining in the Witwatersrand region of South Africa, for example, has severely contaminated ground and surface water with metal-laden acid mine drainage (AMD). Rivers and streams used for potable and agricultural purposes are contaminated, and recent efforts at re-working old dumps for unrecovered gold have exacerbated the problem (Durand 2012; Naicker et al. 2003; Tutu et al. 2008). AMD-contamination of water resources is of concern due to the detrimental effects of excessive metal concentrations (Georgopoulos et al. 2011); their removal from contaminated water is therefore vital.

A number of techniques, including chemical precipitation, bioremediation, adsorption, and ion exchange exist for the removal of metal ions from AMD-contaminated water. Adsorption is widely investigated due to its low costs and the wide range of adsorbents available, including agricultural wastes, fly ash, and activated carbon (Babel and Kurniawan 2003). Lately, the use of nanomaterials as adsorbents has attracted interest because nanomaterials have better reactivity and larger surface area to volume ratios, which facilitate greater adsorption rates and efficiencies (Brown et al. 1999). Engates and Shipley (2011),

Electronic supplementary material The online version of this article (doi:10.1007/s10230-014-0311-7) contains supplementary material, which is available to authorized users.

A. Etale (✉) · D. C. Drake
School of Animal Plant and Environmental Sciences,
University of the Witwatersrand, Private Bag X3,
WITS, Johannesburg 2050, South Africa
e-mail: aetale@gmail.com

H. Tutu
Molecular Sciences Institute, School of Chemistry,
University of the Witwatersrand, Private Bag X3,
WITS, Johannesburg 2050, South Africa

for example, noted that metal adsorption was >5 times faster with titanium dioxide (titania) NPs (8.3 nm) than with bulk particles (329.8 nm).

Nanoparticles (NPs) of various metal oxides, including iron, aluminium, titanium, and manganese have been extensively investigated for metal removal [see review by Hua et al. (2012)]. Silica NPs have also been widely researched (Lee et al. 2011; Michard et al. 1996; Wu et al. 2009). These studies are, however, not applicable to AMD conditions because of the pH at which they were conducted and because relevant ions (e.g. sulphates, ferric, and manganese ions) that could potentially influence adsorption were not studied.

Mesoporous silica NPs are potentially especially appropriate for removing contaminants from AMD for a number of reasons, including their high surface area and low (pH 2–3) pH_{PZC} (Kosmulski 2009), which means that particles are negatively charged at the low pH of AMD (often $\leq$ 3), and primed for cation adsorption. A high surface area translates to higher adsorption efficiencies than bulk counterparts, a requirement for less adsorbent masses, and consequently, generation of lower waste volumes (Engates and Shipley 2011). This is particularly important in light of the challenges currently presented by toxic waste disposal. NPs may also be used in smaller-scale treatment options, e.g. as adsorbents in water filtration devices. Such devices are particularly relevant where large scale pump-and-treat set-ups are uneconomical due to wide geographic dispersal of sources or low volumes of contaminated water, but where treatment is still required due to exposure of populations to contaminated water. In Johannesburg, for example, residents of informal settlements and small farm holdings are reported to drink and cook with water from AMD-contaminated streams and groundwater (Saad et al. 2013). We assessed the sorptive action of mesoporous silica NPs and their suitability for the removal of Cu, Mn, and U from AMD-contaminated waters. U contamination is particularly significant in the Witwatersrand gold fields, with concentrations as high as 72.7 mg L^{-1} (Tutu et al. 2008). Using commercially prepared silica NPs and low pH metal solutions, we quantified the effects of time, metal concentration, NP concentrations, temperature, and Fe^{3+}, Mn^{2+}, and SO_4^{2-} ions on adsorption of these ions. The process was also studied at higher pHs in order to determine process efficiency in pH-amended mine water.

Materials and Methods

The size and morphology of silica NPs (Sigma Aldrich; Schnelldorf, Germany) were investigated by transmission electron microscopy (FEI Tecnai G^2 Spirit TEM). 0.1 g of silica NPs was suspended in 100 mL of deionised water and sonicated for 30 min. A drop of the suspension was then placed on a lacey copper grid and left to dry for 20 min before analysis. Fourier transform infrared (FTIR) spectra of NPs were collected in the 4,000–500 cm^{-1} frequency range on a Bruker Tensor 27 IR spectrophotometer (MA, USA). The specific surface area and porosity of particles were determined by the BET (Brunauer–Emmett–Teller) and BJH (Barret–Joyner–Halenda) methods using a Micrometrics Tristar 3000 porosity analyser (GA, USA).

All metal salts used were analytical grade. Copper nitrate ($Cu(NO_3)_2{\cdot}2.5\ H_2O$) and manganese nitrate ($Mn(NO_3)_2{\cdot}H_2O$) were from Sigma Aldrich (Schnelldorf, Germany). Uranyl nitrate ($UO_2(NO_3)_2{\cdot}6H_2O$), ferric nitrate ($Fe(NO_3)_3{\cdot}9H_2O$), and disodium sulphate (Na_2SO_4) were from Ace Chemicals (Johannesburg, South Africa). Stock metal solutions (1,000 mg L^{-1}) were prepared by dissolving appropriate masses of metal salts in deionised water. NP suspensions (3 mg L^{-1}) were prepared by 30 min water bath sonications. Where necessary, the pH of metal solutions and NP suspensions was adjusted prior to experiments using 0.01 M HNO_3 and 0.01 M NaOH. All experiments were carried out in triplicate, at pH 3.0 ($\pm$0.2) and ambient temperature (25 $\pm$ 2 °C).

Metal adsorption was studied in batch experiments using 13.11 mg Cu L^{-1}, 7.55 mg Mn L^{-1} and 42.18 mg UL^{-1} solutions. Freshly sonicated NP suspensions (10 mL) were reacted with 10 mL metal nitrate solutions in 50 mL polyethylene terephthalate (PET) jars for 60 min. A similar procedure was followed for surface and ground water samples except without pH adjustment. Surface water was collected on two occasions from the Tweelopiespruit, a stream into which a mine shaft decants (26°50′21.67″S, 27°42′57.49″E). The first sampling site was approximately 500 m downstream of the second. Groundwater was from a well 650 m away from the stream (26°05′32.6″S, 27°42′44.6″E).

The effect of contact time was evaluated for durations ranging from 5 s to 60 min. The effects of Fe^{3+}, Mn^{2+}, and SO_4^{2-} ions, introduced as $Fe(NO_3)_3{\cdot}9H_2O$, $Mn(NO_3)_2{\cdot}H_2O$, and Na_2SO_4, respectively, were quantified for 1:1 and 1:2 molar ratios to the test ion. At the end of the experiments, mixtures were filtered and filtrates acidified with 3 mL of 1 % HNO_3. Metal concentrations in filtrates were determined by inductively coupled plasma-optical emission spectrometry (ICP-OES; Kleve, Germany). Adsorption efficiencies were determined by mass balance calculations. The equilibrium adsorption capacity of NPs (q_e; mg g^{-1}) was calculated using Eq. 1 (Lee et al. 2011), where C_i and C_e are the initial and equilibrium ion concentrations (mg L^{-1}), m is the mass of adsorbent (g), and V is the volume of adsorbent solution used (L).

$$q_e = \frac{(C_i - C_e)V}{m} \quad (1)$$

Data Analysis

Kinetics data were fitted to the pseudo-first-order model (Eq. 2) and the pseudo-second-order model (Eq. 3), where q_e and q_t are the NP metal loading capacities (mg g^{-1}) at equilibrium and time t, respectively (Ho and Mckay 2004). The rate constants, k_1, and k_2, were determined from the slope and intercept of the plots of the equations plotted as follows: log ($q_e - q_t$) versus t for the pseudo-first-order model and t/q_t versus t for the pseudo-second-order model.

$$\log(q_e - q_t) = \log q_e - \left(\frac{k_1}{2.303}\right)t \quad (2)$$

$$\frac{t}{q_t} = \left(\frac{1}{k_2}\right) + \left(\frac{1}{q_e}\right)t \quad (3)$$

Isotherm data were fitted to the Langmuir, Freundlich, and Temkin models (LeVan and Vermeulen 1981). The Langmuir model, which best describes monolayer adsorption, is underlain by assumptions such as the absence of adsorbate interactions. Its linear form is given in Eq. 4, where q_{max} is the maximum concentration of metal ions sorbed per unit weight of NPs (mg g^{-1}), and K_L (L mg^{-1}) is the Langmuir constant for the reaction. q_{max} and K_L were determined from the intercept and slope of the plot of C_e/q_e versus C_e.

$$\frac{C_e}{q_e} = \left(\frac{1}{q_{max}}\right) C_e + \left(\frac{1}{K_L q_{max}}\right) \quad (4)$$

The Freundlich model on the other hand, accommodates multi-layer adsorption. It is expressed by Eq. 5, where K_F and $1/n$ are constants specific to each reaction. K_F (mg g) (L $mg)^{1/n}$ is the adsorption value at unit concentration, and $1/n$ is related to the adsorption intensity and heterogeneity of the sorbent surface (Foo and Hameed 2010). These constants were deduced from the intercept and slope, respectively, of a plot of log q_e versus log C_e.

$$\log q_e = \left(\frac{1}{n}\right) \log C_e + \log K_F \quad (5)$$

The Temkin model accounts for the effects of adsorbate interactions excluded by the Langmuir model. It assumes that the heat of adsorption decreases linearly as adsorption increases due to these interactions. It is represented by Eq. 6 where R is the gas constant (8.3145 J mol^{-1} K^{-1}), T is the absolute temperature, b_T is the variation in adsorption energy (J mol^{-1}), and A_T is the equilibrium binding constant (L mg^{-1}). b_T and A_T were deduced from the slope and intercept of a plot of q_e versus ln C_e.

$$q_e = \frac{RT}{b_T} \ln C_e + \frac{RT}{b_T} \cdot \ln A_T \quad (6)$$

The effect of temperature on adsorption at pH 3 was assessed at temperatures ranging from 293 to 310 K. The standard Gibbs free energy (ΔG°) was calculated using Eq. 7 where R is as given above and K is the experimental temperature in Kelvin. K_c was calculated using Eq. 8 where C_{ads} is the adsorbed metal concentration at equilibrium.

$$\Delta G^o = -RT \ln K_c \quad (7)$$

$$K_c = \frac{C_e}{C_{ads}} \quad (8)$$

The standard enthalpy (ΔH°) and entropy (ΔS°) of reactions were then deduced from the slope and intercept of a plot of Van't Hoff's equation (Eq. 9), i.e. ln K_c versus $1/T$.

$$\ln K_c = -\frac{\Delta H^o}{R} \cdot \frac{1}{T} + \frac{\Delta S^o}{R} \quad (9)$$

Results and Discussion

Particle Characterisation

Transmission electron micrographs (Fig. 1) revealed polydisperse porous silica particles with diameters in the <20–50 nm range. The average BET surface area of particles was determined as 612 m^2 g^{-1} and the average pore diameter as 4 nm, indicating that the particles were mesoporous (Sing et al. 1985). FTIR spectra (data not shown) consisted of two distinct frequency regions: 4,000–2,500 nm and 1,700–400 nm, which confirmed the silica composition of the NPs, i.e. a broad adsorption band in the 4,000–2,500 nm region due to O–H vibrations from

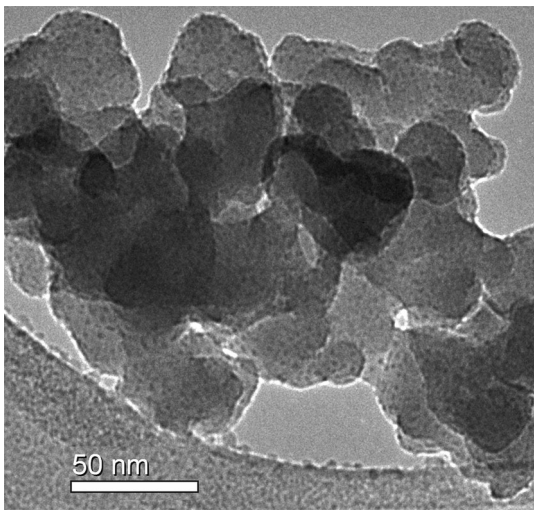

Fig. 1 **a** Transmission electron micrograph of silica NPs

adsorbed or molecular water and one in the 1,700–400 nm range due to Si–OH vibration and stretching modes (Swann and Patwardhan 2011).

Effect of Adsorbent Concentration

The optimal adsorbent concentration for experiments was determined by reacting metal solutions with 1, 3, 5, and 9 mg L^{-1} of silica NP suspensions for 60 min. The results (Fig. 2) show that adsorbed metal concentrations increased and then decreased, albeit slightly, with increasing adsorbent concentrations.

A number of NP properties affect the behaviour of NPs in aqueous media, and subsequently, their adsorption efficiency. For example, as opposed to larger adsorbents whose sorption efficiencies tend to increase with adsorbent concentration, metal adsorption with silica NPs was reduced at NP concentrations greater than 3 mg L^{-1}. This is likely due to NP agglomeration, which reduces access to sorption sites. NP agglomeration in aqueous media occurs as the result of the high surface energies of NPs. The process is affected by, among other things: NP concentrations, i.e. higher concentrations increase the chances of collisions and; solution pH, i.e. NP coalescence increases as solution pH approaches the pH_{PZC} because of reduction in repulsive surface charges (Guzmán et al. 2006). With a pH_{PZC} of pH 2, silica NPs were likely considerably agglomerated and increasing their concentration only served to increase agglomeration, hence the lower adsorption. Optimal adsorption for all three metals corresponded with an NP concentration of 3 mg L^{-1}; this NP concentration was therefore used in subsequent experiments.

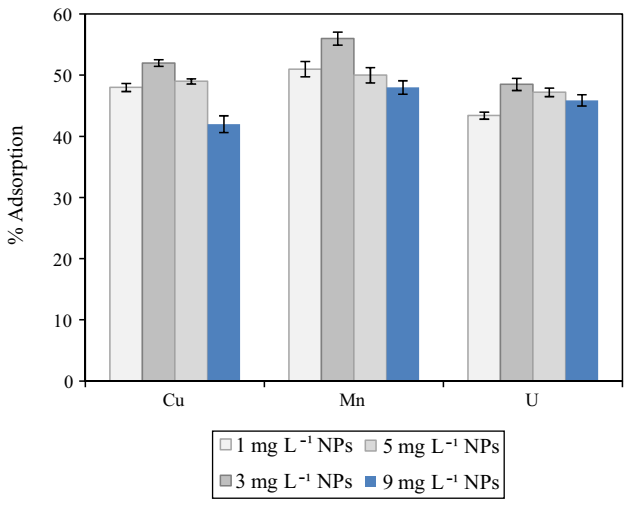

Fig. 2 The effect of adsorbent concentration on adsorption of Cu, Mn and U to silica NPs at pH 3 (±SD)

Effect of Contact Time

The effect of contact time on adsorption was studied at time durations ranging from five s to 60 min. Reactions were rapid and equilibrium was attained in 5 min for Cu and within a minute for Mn and U (Fig. 3). Rapid adsorption rates were also reported in other investigations, including those of Akhbarizadeh et al. (2013) and Lee and Yi (2007). Brown et al. (1999) proposed that this phenomenon is due to the higher number of surface atoms and defects such as kinks and edges that are more reactive.

Kinetics data were better described by the pseudo second-order model than the pseudo-first-order model (Table 1). The highest initial adsorption rate (h) and equilibrium adsorption concentration (q_e) were recorded for U due to greater mass transfer action from higher initial concentrations (Ho and Mckay 2004). However, the overall adsorption rate (k_2), was highest for Mn, despite the fact that higher concentrations of Cu and U should have resulted in greater driving forces and faster rates for Cu and U. Indeed, the Mn adsorption rate was >3 times faster than that of Cu and 7 times faster than that of U. We surmise that the structural configuration of sorption sites on NP surfaces was more favourable to Mn ions than Cu and U. This hypothesis was put forward by Madden and Hochella (2005), who found that certain binding environments stabilized the distorted octahedron of Mn^{3+} relative to the perfect octahedron of Mn^{2+}. Thus, steric hindrances and configurational disadvantages may have slowed down the adsorption of Cu and U to sorption sites, and eventually reduced their equilibrium adsorption efficiencies.

Effect of Initial Metal Concentrations

The adsorption capacity of silica NPs at pH 3 was studied using metal concentrations ranging from 13.11 to

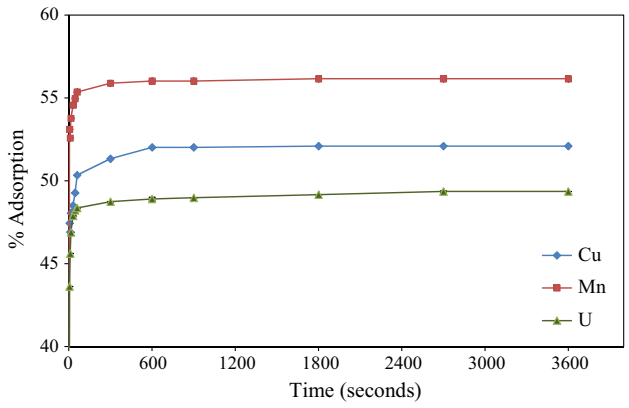

Fig. 3 The effect of contact time on the adsorption of Cu, Mn and U by silica NPs (±SD)

Table 1 Adsorption rate constants and coefficients of correlation (R^2) for kinetics models fitted to adsorption data

Metal	Initial concentration (mg L^{-1})	Pseudo-second order model				Pseudo-first order model
		R^2	k_2 (mg g^{-1} s^{-1})	h (mg g^{-1} s^{-1})	q_e (mg g^{-1})	R^2
Cu	13.11	1	0.02	11.99	22.78	0.75
Mn	7.55	1	0.07	14.04	14.14	0.74
U	42.18	1	0.01	28.57	69.44	0.89

127 mg L^{-1} for Cu, 7.55 to 84 mg L^{-1} for Mn and 4.46 to 464 mg L^{-1} for U. For all three, equilibrium NP loading (q_e) increased with initial metal concentrations (Fig. 4). As noted earlier, this was due to greater driving forces at higher initial concentrations for mass transfer to the adsorbent surface (Ho and Mckay 2004).

Isotherm data were better described by the Freundlich and Temkin models (Table 2). The following conclusions can therefore be made concerning the adsorption of test ions to silica NPs: (1) sorption sites on the silica surface were energetically heterogeneous; (2) metal ions formed more than one layer on the silica surface; (3) adsorbate–adsorbate interaction influenced adsorption, and; (4) the adsorption energy decreased linearly with increasing adsorption. In addition, K_F values revealed that, under the experimental conditions, the sorption capacity of silica NPs was much lower for U than Cu and Mn. This is largely a factor of space utilization by adsorbed ions. With a diameter of 6.5 Å (Krestou et al. 2003), the hydrated U ion occupies more space than Cu (4.19 Å) and Mn (4.38 Å) ions (Nightingale 1959). It is also noteworthy that adsorption of Mn exceeds that of Cu, the smaller size of the latter ion notwithstanding. A possible explanation for this has already been mentioned. With respect to $1/n$ values, the <1 values for Cu and Mn imply chemisorption processes for these ions. The >1 $1/n$ value for U, in contrast, is indicative of a cooperative removal processes, i.e. adsorption and precipitation (Foo and Hameed 2010); this conclusion is corroborated by the findings of Michard et al. (1996).

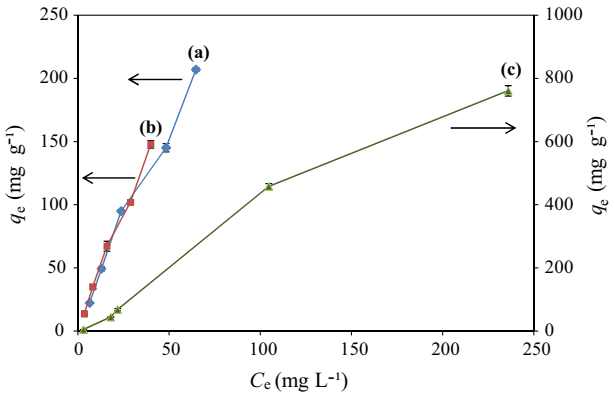

Fig. 4 The effect of initial metal concentration on adsorption of Cu (**a**), Mn (**b**) and U (**c**) (±SD) by silica NPs

Effects of Fe^{3+}, Mn^{2+}, and SO_4^{2-} Ions

The effects of Fe^{3+}, Mn^{2+}, and SO_4^{2-} ions on the adsorption of Cu, Mn^{2+}, and U were investigated at pH 3. The effects of all three additional ions were tested for Cu and U, but only Fe^{3+} and SO_4^{2-} effects were investigated for Mn. Ferric and sulphate ions increased the adsorption of all three test ions in the order U > Cu > Mn (Fig. 5a, b). The effect of Mn ions was, however, varied, i.e. increasing U adsorption in both equimolar and 1:2 systems, but inhibiting Cu adsorption in 1:2 Cu/Mn systems (Fig. 5c).

To explain these observations, metal speciation at variable pH was deduced using MEDUSA software (KTH Royal Institute of Technology 2004). Results indicated that Cu formed a $CuFe_2O_4$ precipitate in the presence of ferric ions (supplemental Figure 1a), to which the increase in Cu removal may be ascribed. However, no complex was formed with Mn and U. The slight increases in adsorption may be due to additional sorption sites availed by the Fe_2O_3 phase (supplemental Figure 1b). [Supplemental figures accompany the on-line version of this paper, which can be downloaded for free by all journal subscribers]. Sulphates, on the other hand, likely enhanced adsorption by lowering the energy barrier for the approach of ions to the adsorbent surface (James and Healy 1972b) or the formation of more adsorbable species (Benjamin and Leckie 1982). Kosmulski (1999) also suggested that when anion concentrations are higher than metal concentrations, adsorption may be enhanced by the formation of ternary surface complexes.

With respect to Mn and its concentration-dependent effects on Cu sorption, we surmise that both ions sorb to similar sites on the silica surface (Benjamin and Leckie 1981). Competition for sorption sites thus ensued in mixed solutions, and Cu sorption was inhibited due to the faster sorption rate and possible configurational advantages of Mn (see earlier discussion). Inhibition is, however, not evident in equimolar solutions due to availability of sorption sites.

Table 2 Parameters of adsorption isotherms fitted to adsorption data

Metal	Freundlich isotherm			Temkin isotherm			Langmuir isotherm
	R^2	K_F (mg g^{-1}) (L $mg^{-1})^{1/n}$	$1/n$	R^2	A_T (L g^{-1})	b_T (MJ mol^{-1})	R^2
Cu	0.99	4.06	0.95	0.95	1.58×10^4	1.9	0.60
Mn	0.99	4.45	0.95	0.92	2.46×10^4	2.5	0.44
U	0.99	1.44	1.19	0.83	6.91×10^4	3.2	0.28

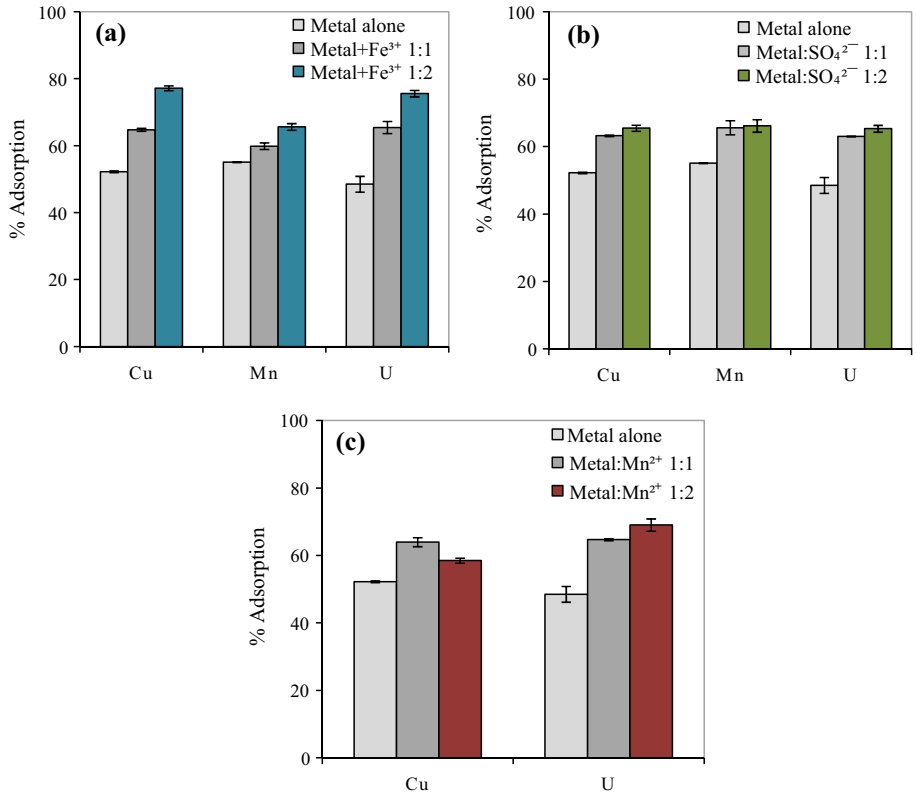

Fig. 5 The effect of Fe^{3+} (**a**), SO_4^{2-} (**b**) and Mn^{2+} (**c**) ions on the adsorption of Cu, Mn and U by silica NPs (±SD) at pH 3

Effect of pH

Adsorption was studied at higher pH in order to determine the efficiency of the process in contaminated waters whose pH has been amended intentionally or by natural processes. Adsorption of all three ions increased with solution pH (Fig. 6). Copper adsorption increased from 52 % at pH 3 to 94 and 99 % at pH 7 and 9, respectively. Increases in Mn adsorption, on the other hand, were modest: only 5.7 % across the test pH range. The maximum adsorption of U (77 %) was recorded at pH 7 and 9 due to the dominance of $(UO_2)_2(OH)_2^{2+}{\cdot}H_2O$ in solution above pH 6.

As reported by James and Healy (1972a) and Krestou et al. (2003), increases in adsorption coincided with the onset of hydrolysis and the formation of more adsorbable species like $Cu(OH)_2$ and $UO_2(OH)_2$. Removal of all three ions was also influenced by declining competition from H^+ ions as pH increased. Solution pH also influenced adsorbent properties, i.e. (1) the silica surface became more negatively charged and thus favourable for cation adsorption; (2) NPs experienced less aggregation resulting in greater

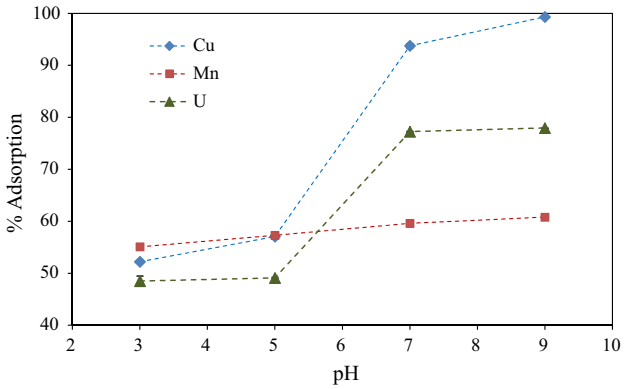

Fig. 6 The effect of pH on adsorption of Cu, Mn and U to silica NPs (±SD)

Table 3 Thermodynamic parameters for the adsorption of Cu, Mn and U to silica NPs

Metal	$\Delta G°$ (kJ mol^{-1})				$\Delta H°$ (kJ mol^{-1})	$\Delta S°$ (J mol^{-1} K^{-1})	R^2
	293 K	298 K	303 K	310 K			
Cu	−3.38	−3.69	−3.91	−4.33	18.32	9.01	0.99
Mn	−4.17	−4.39	−4.61	−4.95	15.26	8.09	0.99
U	−0.02	−0.42	−0.73	−1.15	21.95	9.03	0.99

access to sorption sites (Guzmán et al. 2006), and; (3) increased silica dissolution increased the population of available sorption sites (Kosmulski 2000). Indeed, changes in adsorbent surface properties may be responsible for the slight increases in Mn adsorption since it did not hydrolyze in the test pH range. Hydrolysis does not, however, guarantee maximum adsorption. Krestou et al. (2003) suggested that U adsorption may not attain high efficiencies due to the non-adsorption of poly-nuclear species like $(UO_2)_2(OH)_2^{2+}$ and $(UO_2)_3(OH)_5^{+}$, and uranyl carbonate species. Sorption efficiencies presented here are similar to those reported by Štamberg et al. (2003) in the presence of carbonates (75 %) and although they do not attain the 95 % removal efficiencies of carbonate-free systems, they provide a more accurate picture for in situ operations.

Effect of Temperature

The effect of temperature on adsorption was investigated at 293, 298, 303, and 310 K. Adsorption increased with temperature from 49 to 58 % for Cu, 54 to 61 % for Mn, and 45 to 56 % for U, implying that adsorption of these ions to sites on the silica surface is an endothermic process (Table 3). $\Delta G°$ values were negative, indicating that adsorption was spontaneous and thermodynamically favourable. The increasing negativity of $\Delta G°$ with temperature also indicates increased adsorption at higher temperatures. The positive $\Delta S°$ and $\Delta H°$ values corroborate the findings on the spontaneity and endothermic nature of adsorption reactions. Similar results were reported for adsorption of Cu and Mn to kaolinite (Yavuz et al. 2003) and U to tin oxide NPs (Nilchi et al. 2013).

Adsorption Mechanism

Adsorption takes place in a number of stages including the transfer of solute molecules from the bulk solution to the exterior of the adsorbent surface, film diffusion, and adsorption to sites on the exterior surface and within pores. Solute transfer in bulk solution is generally a rapid process while film diffusion likely controls the adsorption rate only during the early stages of the reaction. In porous sorbents such as the one used here, transport to sorption sites within pores likely controls the adsorption rate. To investigate the possibility of this, kinetics data were fitted to the intraparticle diffusion model of Weber and Morris (1963) (Eq. 10) where the intraparticle diffusion rate, k_{ipd} (mg g^{-1} s$^{0.5}$) is determined from the slope of a plot of q_t versus $t^{0.5}$. If intraparticle diffusion is the only rate controlling step, the intercept (C) is at the origin. Where $C > 0$, both external mass transfer and pore-diffusion control the adsorption rate.

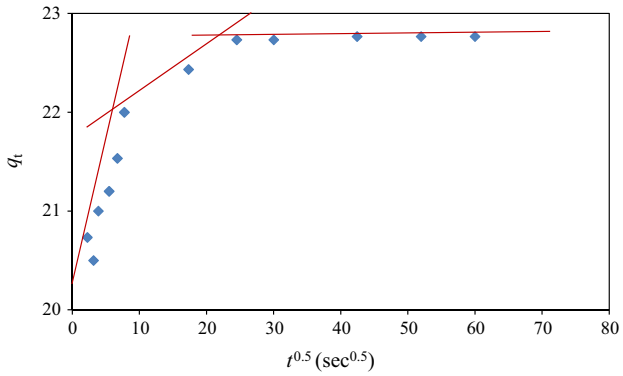

Fig. 7 Intraparticle diffusion plot for adsorption of Cu to silica NPs at pH 3

$$q_t = k_{ipd} \cdot (t^{0.5}) + C \quad (10)$$

Figure 7 shows the plot for Cu; Mn and U plots were similar. Tri-linearity is evident, indicating a three-step adsorption. The first steep linearity can be assigned to external surface adsorption, the second to intraparticle diffusion, and the third to the equilibrium stage (Ramadan et al. 2010). As the second line does not pass through the origin, intraparticle diffusion is not the sole rate-controlling step. Such a conclusion is plausible because access of the hydrated test ions would not be impeded by NP pores with a diameter of 4 nm. Overall adsorption rates, therefore, were determined both by external mass transfer and intraparticle diffusion.

Application Studies

Silica NPs were then applied for the removal of these three ions from field samples of AMD-contaminated surface and ground water. The physical and chemical characteristics of the surface water samples (SW1 and SW2) and the

Table 4 Physico-chemical characteristics of contaminated water used in application studies

Sample	pH	Conductivity (mS cm^{-1})	Redox potential (mV)	$[Cu]_{tot}$ mg L^{-1} (SD)	$[Mn]_{tot}$ mg L^{-1} (SD)	$[U]_{tot}$ mg L^{-1} (SD)
SW1	3.13	3.52	209.0	1.44 (0.003)	49.74 (0.002)	b.d
SW2	2.79	3.87	227.7	1.22 (0.046)	16.48 (0.006)	b.d
GW	5.62	2.76	6.9	0.24 (0.001)	15.00 (0.140)	b.d

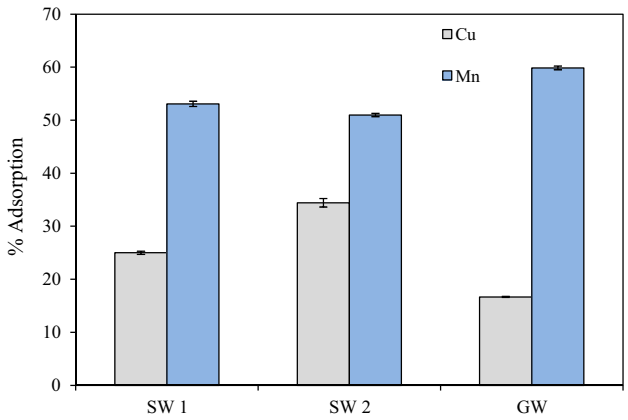

Fig. 8 Removal efficiencies of Cu and Mn from contaminated surface and groundwater by silica NPs; U concentrations were below detection limits

groundwater sample (GW) are presented in Table 4. The chemical signatures of SW1 and SW2 are variable, likely due to dilution from rainfall shortly before the SW2 sample was collected.

The results of adsorption experiments are shown in Fig. 8. Just as with experiments using simulated AMD, more Mn than Cu was adsorbed. This further strengthens the hypothesis that Cu and Mn bind to similar sites on silica. Competition for sorption sites, however, also depends on aqueous concentrations and therefore more Mn was adsorbed due to its higher concentrations. Cu adsorption was higher in the SW2 than SW1 sample due to the lower Cu:Mn ratio in the former (Table 4). The lowest Cu adsorption was in GW where the Mn concentration was 63 greater than the Cu concentration.

Mn removal is often challenging because its late hydrolysis necessitates copious amounts of lime (CaO) for pH adjustment (Johnson and Hallberg 2005). Silica NPs offer an alternative that circumvents the need for prior pH adjustment and, depending on the initial concentrations, low Mn concentrations may be achieved in a few adsorption cycles.

Cost Assessment

A number of techniques are available for the treatment of AMD (see Johnson and Hallberg 2005). In the Central Witwatersrand Basin, a pump-and-treat facility costing approximately USD 30 million has recently been installed by Central Rand Gold to lower the water table to improve access to deeper mining and to treat AMD issuing from the void (Kolver 2014). This plant is designed to treat 84 million L of AMD per day. Both pumping and the high density sludge process used by this plant are energetically demanding, and the approach is likely only competitive because it includes the financial incentive of expanded mining access. This facility cannot be used to treat contamination in the many other AMD-contaminated surface and groundwater bodies around the metropolis due to their low water volumes, dispersed geographical locations, and the considerable costs that would be involved in collecting such waters to a single treatment facility.

Compared to reverse osmosis and distillation, adsorption using nanomaterials, zeolites, and ion-exchange resins is a viable, effective, and relatively low-cost option for household and community-scale treatment of metal-contaminated water (Meridian Institute 2006; supplemental Table 1). Although nanomaterials are more costly than zeolites (0.5–4.50 USD/kg) and ion-exchange resins (42 USD/kg), they are likely more efficient due to their higher surface areas. Among nanomaterials, silica NPs have several advantages, including stability and higher adsorption at low pH, as well as not suffering from corrosion and passivation like the more commonly used nano zero valent iron (n-ZVI). At 1,500 USD/kg, silica NPs are also less costly than an already commercialized product using ferric oxide, which costs 4,500 USD/kg (supplemental Table 1). In this work, 3 mg of silica NPs treated a litre of AMD. The NPs were purchased at R885 (75 USD) for a 50 g bottle. Thus, 50 g should clean 16,667 L, which translates to 0.5 US cents per litre of cleaned water (adsorbent-only cost). This cost should decrease once larger quantities of the material are purchased, due to economies of scale.

These nanoscale adsorbents can also be functionalised and used to target potentially valuable metals, which can then be recovered when filter columns are replaced. The use of silica NPs for treatment of AMD-contaminated water therefore has potentially enormous and multi-faceted economic and social benefits.

Conclusions

We studied the adsorption of Cu, Mn, and U by mesoporous silica NPs with the aim of determining their

applicability for the treatment of AMD-contaminated waters. Results indicate that silica NPs can indeed be used for the adsorptive removal of Cu, Mn, and U from contaminated water at pH 3. Adsorption rates were rapid, implying that metal removal in systems with fast flow-through rates would be successful. However, Cu removal was inhibited by high concentrations of Mn, so repeated adsorption cycles or the modification of silica NP surfaces by functionalities with high affinity for Cu, e.g. amine groups, may be required to attain significant Cu removal in water with high Mn levels. Silica NPs present opportunities for low-cost, efficient provision of clean, potable water from AMD-contaminated sources, as well as potential for the selective recovery of some metals.

Acknowledgments Funding for this work was provided by the Global Change and Sustainability Research Institute (GCSRI) of the University of Witwatersrand in the form of a Ph.D. fellowship to A.E. We acknowledge the contributions of Kirstin Olsen with field sampling, Siyethemba Mabaso with ICP-OES analyses, and Jacques Gerber of the Microscopy and Microanalysis Unit.

References

Akhbarizadeh R, Shayestefar MR, Darezereshki E (2013) Competitive removal of metals from wastewater by maghemite nanoparticles: a comparison between simulated wastewater and AMD. Mine Water Environ 33:89–96. doi:10.1007/s10230-013-0255-3

Babel S, Kurniawan TA (2003) Low-cost adsorbents for heavy metals uptake from contaminated water: a review. J Hazard Mater 97:219–243. doi:10.1016/S0304-3894(02)00263-7

Benjamin MM, Leckie JO (1981) Competitive adsorption of Cd, Cu, Zn, and Pb on amorphous iron oxyhydroxide. J Colloid Interface Sci 83:410–419. doi:10.1016/0021-9797(81)90337-4

Benjamin MM, Leckie J (1982) Effects of complexation by Cl, SO_4 and S_2O_3 on adsorption behaviour of Cd on oxide surfaces. Environ Sci Technol 16:162–170. doi:10.1021/es00097a008

Brown GE, Henrich VE, Casey WH, Clark DL, Eggleston C, Felmy A, Goodman DW, Grätzel M, Maciel G, McCarthy MI, Nealson KH, Sverjensky DA, Toney MF, Zachara JM (1999) Metal oxide surfaces and their interactions with aqueous solutions and microbial organisms. Chem Rev 99:77–174. doi:10.1021/cr980011z

Durand JF (2012) The impact of gold mining on the Witwatersrand on the rivers and karst system of Gauteng and North West Province, South Africa. J Afr Earth Sci 68:24–43. doi:10.1016/j.jafrearsci.2012.03.013

Engates KE, Shipley HJ (2011) Adsorption of Pb, Cd, Cu, Zn, and Ni to titanium dioxide nanoparticles: effect of particle size, solid concentration, and exhaustion. Environ Sci Pollut Res Int 18:386–395. doi:10.1007/s11356-010-0382-3

Foo KY, Hameed BH (2010) Insights into the modeling of adsorption isotherm systems. Chem Eng J 156:2–10. doi:10.1016/j.cej.2009.09.013

Georgopoulos PG, Roy A, Opiekun RE, Lioy PJ (2011) Environmental copper: its dynamics and human exposure issues. J Toxicol Environ Heal B 4:341–394. doi:10.1080/10937400173146207

Guzmán KAD, Taylor MR, Banfield JF (2006) Environmental risks of nanotechnology: national nanotechnology initiative funding, 2000–2004. Environ Sci Technol 40:1401–1407. doi:10.1021/es0515708

Ho YS, Mckay G (2004) Sorption of copper(II) from aqueous solution by peat. Water Air Soil Pollut 158:77–97. doi:10.1023/B:WATE.0000044830.63767.a3

Hua M, Zhang S, Pan B, Zhang W, Lv L, Zhang Q (2012) Heavy metal removal from water/wastewater by nanosized metal oxides: a review. J Hazard Mater 212:317–331. doi:10.1016/j.jhazmat.2011.10.016

James RO, Healy TW (1972a) Adsorption of hydrolyzable metal ions at the oxide-water interface. I. Co(II) adsorption on SiO_2 and TiO_2 as model systems. J Colloid Interface Sci 40:42–52. doi:10.1016/0021-9797(72)90174-5

James RO, Healy TW (1972b) Adsorption of hydrolyzable metal ions at the oxide-water interface. III. A thermodynamic model of adsorption. J Colloid Interface Sci 40:65–81. doi:10.1016/0021-9797(72)90174-9

Johnson DB, Hallberg KB (2005) Acid mine drainage remediation options: a review. Sci Total Environ 338:3–14. doi:10.1016/j.scitotenv.2004.09.002

Kolver L (2014) Central Rand Gold Mill 3 operational, AMD treatment started. In: Eyewitness news http://ewn.co.za/BusinessData/CRG%20Mill%203%20operational_%20AMD%20treatment%20started%20_%20Leandi%20Kolver. Accessed 17 July 2014

Kosmulski M (1999) Adsorption of trivalent cations on silica. J Colloid Interface Sci 211:410–412. doi:10.1006/jcis.1998.6034

Kosmulski M (2000) Sorption of heavy metal cations on silica. In: Papirer E (ed) Adsorption on silica surfaces. Marcel Dekker, New York, pp 399–437

Kosmulski M (2009) pH-dependent surface charging and points of zero charge. IV. Update and new approach. J Colloid Interface Sci 337:439–448. doi:10.1016/j.jcis.2009.04.072

Krestou A, Xenidis A, Panias D (2003) Mechanism of aqueous uranium (VI) uptake by natural zeolitic tuff. Miner Eng 16:1363–1370. doi:10.1016/j.mineng.2003.08.012

KTH Royal Institute of Technology (2004) HYDRA/MEDUSA

Lee H, Yi J (2007) Removal of copper ions using functionalised mesoporous silica in aqueous solution. Sep Sci Technol 36:2433–2448. doi:10.1081/SS-100106101

Lee HW, Cho HJ, Yim JH, Kim JM, Jeon JK, Sohn JM, Yoo KS, Kim SS, Park YK (2011) Removal of Cu(II)-ion over amine-functionalized mesoporous silica materials. J Ind Eng Chem 17:504–509. doi:10.1016/j.jiec.2010.09.022

LeVan MD, Vermeulen T (1981) Binary langmuir and freundlich isotherms for ideal adsorbed solutions. J Phys Chem 85:3247–3250. doi:10.1021/j150622a009

Madden A, Hochella M (2005) A test of geochemical reactivity as a function of mineral size: manganese oxidation promoted by hematite nanoparticles. Geochim Cosmochim Acta 69:389–398. doi:10.1016/j.gca.2004.06.035

Meridian Institute (2006) Overview and comparison of conventional treatment technologies: nano-based treatment technologies. In: Proceedings of the international workshop on nanotechnology, water, and development, pp 7–38. http://www.merid.org/~/media/Files/Projects/nano-waterworkshop/watertechpaper.ashx

Michard P, Guibal E, Vincent T, Le Cloirec P (1996) Sorption and desorption of uranyl ions by silica gel: pH, particle size and porosity effects. Microporous Mater 5:309–324. doi:10.1016/0927-6513(95)00067-4

Naicker K, Cukrowska E, McCarthy TS (2003) Acid mine drainage arising from gold mining activity in Johannesburg, South Africa and environs. Environ Pollut 122:29–40. doi:10.1016/S0269-7491(02)00281-6

Nightingale ER (1959) Phenomenological theory of ion solvation. Effective radii of hydrated ions. J Phys Chem 63:1381–1387. doi:10.1021/j150579a011

Nilchi A, Dehaghan T, Garmarodi S (2013) Kinetics, isotherm and thermodynamics for uranium and thorium ions adsorption from aqueous solutions by crystalline tin oxide nanoparticles. Desalination 321:67–71. doi:10.1016/j.desal.2012.06.022

Nriagu JO (1988) A silent epidemic of environmental metal poisoning? Environ Pollut 50:139–161. doi:10.1016/0269-7491(88)90189-3

Ramadan H, Ghanem A, El-rassy H (2010) Mercury removal from aqueous solutions using silica, polyacrylamide and hybrid silica—polyacrylamide aerogels. Chem Eng J 159:107–115. doi:10.1016/j.cej.2010.02.051

Saad DM, Cukrowska EM, Tutu H (2013) Selective removal of mercury from aqueous solutions using thiolated cross-linked polyethylenimine. Appl Water Sci 3:527–534. doi:10.1007/s13201-013-0100-7

Sing KSW, Everett DH, Haul RA, Moscou L, Pierotti RA, Rouquerol J, Siemieniewska T (1985) Reporting physisorption data for gas/solid systems. Pure Appl Chem 57:603–619. doi:10.1002/9783527610044.hetcat0065

Štamberg K, Venkatesan KA, Vasudeva Rao PR (2003) Surface complexation modeling of uranyl ion sorption on mesoporous silica. Colloid Surf A 221:149–162. doi:10.1016/S0927-7757(03)00139-0

Swann GEA, Patwardhan SV (2011) Application of Fourier transform infrared spectroscopy (FTIR) for palaeoenvironmental research. Clim Past 65–74. doi:10.5194/cp-7-65-2011

Tutu H, McCarthy TS, Cukrowska E (2008) The chemical characteristics of acid mine drainage with particular reference to sources, distribution and remediation: the Witwatersrand Basin, South Africa as a case study. Appl Geochem 23:3666–3684. doi:10.1016/j.apgeochem.2008.09.002

Weber JW, Morris JC (1963) Kinetics of adsorption on carbon from solutions. J Sanit Eng ASCE 89(2):31–60

Wu S, Li F, Xu R, Wei S, Li G (2009) Synthesis of thiol-functionalized MCM-41 mesoporous silicas and its application in Cu(II), Pb(II), Ag(I), and Cr(III) removal. J Nanoparticle Res 12:2111–2124. doi:10.1007/s11051-009-9770-3

Yavuz O, Altunkaynak Y, Güzel F (2003) Removal of copper, nickel, cobalt and manganese from aqueous solution by kaolinite. Water Res 37:948–952. doi:10.1016/S0043-1354(02)00409-8